IEEE Access
Multidisciplinary ⋮ Rapid Review ⋮ Open Access Journal

Received 22 November 2022, accepted 12 December 2022, date of publication 14 December 2022,
date of current version 20 December 2022.

Digital Object Identifier 10.1109/ACCESS.2022.3229212

RESEARCH ARTICLE

Spatial Changes of Ocean Circulation Along the Coast of Gulf of Thailand Using Tide Gauge Measurements

KUTUBUDDIN ANSARI[1], JOSÉ FRANCISCO DE OLIVEIRA-JÚNIOR[2], AND PUNYAWI JAMJAREEGULGARN[3]

[1]Integrated Geoinformation (IntGeo) Solution Private Ltd., New Delhi 110025, India
[2]Institute of Atmospheric Sciences (ICAT), Federal University of Alagoas (UFAL), Maceió, Alagoas 57072-260, Brazil
[3]King Mongkut's Institute of Technology Ladkrabang, Prince of Chumphon Campus, Chumphon 86160, Thailand

Corresponding author: Punyawi Jamjareegulgarn (kjpunyaw@gmail.com)

ABSTRACT The study presents linear and nonlinear (smoothing spline) modeling of sea-level measurements on the basis of 50-year (1971-2020 A.D.) permanent service for mean sea-level (PSMSL) tide gauge data at the coastal area of the Gulf of Thailand. These tide gauge measurements are compared with the ORAS5 data extracted from the latest ECMWF atmospheric reanalysis-ERA5. The comparative analyses showed that both kinds of data are correlated with a correlation coefficient of more than 0.94. Moreover, to examine the performance and the complexity of tide gauge measurements at each site, the multitaper spectral analysis is carried out and the spectral estimates are also estimated. Our spectral analyses showed that the sea-level measurements at each site have different levels of fluctuation because of individual local influence. The proposed multitaper spectral analysis can be considered as an appropriate method for tide gauge analysis and can be applied to attain the fluctuation of sea-level at the global level.

INDEX TERMS Gulf of Thailand, PSMSL, ORAS5, nonlinear modeling, tile gauge measurement.

I. INTRODUCTION

The global rate of sea-level rising in the last few decades has been argued by several authors on the basis of tide gauge measurements [1], [2], [3], [4]. These observed sea-level variation at any place in the world depends upon several factors such as seasonal cycle, interannual secular variability, surge, geological and interglacial variations, and astronomical components [5], [6]. Sea-level variability for long-term period, especially the sea-level rising, is important to study not only for society or coastal management, but also for the global warming manifestation [7], [8], [9]. Previous studies based on satellite altimeter and tide gauge observations revealed that the global sea-level rising was around 1.31 cm/year during the last period of the 20th century [10], [11], [12]. The sea-level tended to rise in the eastern Indian Ocean and western Pacific Ocean while tending to fall in the western Indian Ocean and eastern Pacific Ocean [11], [13]. The overall sea-level change is not uniform all over the world, because the changes in upper oceanic circulations in response to the surface winds forcing induce the spatial dependency of oceanic water level variation [14], [15], [16]. The oscillation of sea-level is well known in time following many periodicities associated with both the measured length record and the detectable longest periodicity [9], [17]. The tide gauge measurements of sea-level are not the absolute sea-level, because the land keeps on moving downward or upward due to the subsidy and the isostasy. The change of instrument or its relocation work may also reduce the quality of records. In this way, the absolute measurement of sea-level change is difficult, however, the relative change of sea-level has been derived mainly from the tide gauge measurement relative to the fixed tide gauge benchmarks. This relative sea-level change referred to the total sum of sea-level changes as well as subsidence and uplift changes in the land [8].

Numerous studies have recorded the rise of global sea-level with distressing physical, social and economic impacts

The associate editor coordinating the review of this manuscript and approving it for publication was Abdel-Hamid Soliman.

on the coastal societies [18], [19], [20], [21]. Therefore, such studies have tried to protect the lives and the properties of humans from natural disasters such as inundation and flooding due to the fluctuation of sea-level in coastal zones. Kang and Lin [22] studied wavelet analysis by using three types of hydrological data like precipitation, water level, and stream flow. They noticed some temporal patterns in water level and stream flow, while there was nothing in the case of precipitation. Hidayat et al. [23] used both the upstream water and the tide level data in conjunction with the artificial neural network models to predict the tidal river discharge. The obtained results showed up to two days of advanced good performance. Lee et al. [24] first separated the wave and tide components by using curve fitting and wavelet analysis, then a high pass filter was used to distinguish the noise and rainfall-induced runoff components at the respective time series. Afterwards, Balogun and Adebisi [25] predicted the ocean-atmospheric variables along with the Malaysian coastline by using deep learning and machine learning techniques. The four-variable combinations (i.e., sea surface atmospheric pressure, temperature, density, and salinity) are used to investigate along with the precipitation, the net cloud cover, the wind speed, and the sea-level data, as well as train the SVR, ARIMA, LSTM, and neural network models. As for their analyses, they noticed that the prediction accuracy of atmospheric processes is more influential as compared to the oceanic processes. In their analysis by a heat map, it has been deduced that the atmospheric pressure at the surface and the mean sea level pressure have equal influence on the sea level anomaly with a correlation value of 0.15. This kind of similar pattern was for all stations. Hence, sea level pressure was excluded for further processing to avoid collinearity issues. Deepa and Gnanaseelan [26] also studied the decadal sea-level variability of Indian Ocean using long-term tide gauge measurements observed at seventeen stations. They revealed that a close association between the sea-level of Indian Ocean and other global decadal climate models such as the Pacific Decadal Oscillation and Atlantic Multidecadal Oscillation can be observed successfully. Piscopo et al. [27] focused on the sea-wave measurements and their analysis. They described a brief review of the most common propagation and generation of oceanic waves. Subsequently, they discussed the sea-waves spectral analysis on the basis of the most promising methods which allowed to obtain the sea-state parameters beginning from the time history of wave elevation.

Although several studies have been proposed to carry out the oceanic circulations around the world, we find a space gap in the literature for the Gulf of Thailand. The Gulf of Thailand is located in the southwestern South China Sea, bordered by Thailand, Cambodia, Vietnam, and Malaysia. The length and the width of the Gulf of Thailand are around 800 km and 560 km, respectively, with a surface area of around 320,000 km^2 from 6°N to 13.50°N latitudes and 99°E to 104°E longitudes. The Gulf of Thailand is a shallow bay where the average depth is around 58 m and the maximum depth is around 85 m. Because the shallow depth exchange of water in the gulf is slow, the strong inflow of water from rivers enriches the sediments and reduces the salinity (3.05–3.25%) in the gulf. Moreover, the rivers which empty mainly into the gulf include Chao Phraya River, Bang Pakong River, Tha Chin River, Mae Klong, and Tapi River. The objective of this research is to analyze the sea-level observations around the Gulf of Thailand and to investigate the surge heights, astronomical tidal constituents, sea-level patterns, and the characteristics of its components. This present work contributes a better sense of experimentally determined sea-level patterns in the Gulf of Thailand. Additionally, the purpose of this study is to explain the variability of sea-level along the coastal area of the Gulf of Thailand with response to the large-scale changes in oceanic circulations using tide gauge measurements.

II. TIDE GAUGE MEASUREMENTS AND METHOD OF ANALYSIS

The whole study has been divided in flowing three steps:

A. ANALYZING THE PSMSL TIDE GAUGE

In the first step, we used the monthly PSMSL mean sea-level observation obtained from six stations (https://www.psmsl.org/data/obtaining/) for 50 years (1971 - 2020 A.D.) along the coastal area of the Gulf of Thailand as shown in Fig. 1 and Table 1. The Permanent Service for Mean Sea Level (PSMSL), established in 1933, are responsible for the data collection, analysis, and interpolation of the sea-level measurements from the global network of tide gauge. Previously, a tide gauge was installed at the seaports to operate commercial vessels and to reduce flooding and erosion. Initially, it was not intended to measure the sea-level which was first used for this purpose in the early 20th century [28]. The tide gauge distribution is controlled by the site's inadequate coverage of open sea and islands [29], [30]. The study also includes earthquake catalogs from 2005 to 2020 (the seismic data was not available before 2005) managed by the European–Mediterranean Seismological Centre (EMSC; https://www.emsc-csem.org/Earthquake/) as shown in Fig. 1 and Table 2. There were only three earthquake events that were noticed from the year 2005 to 2020 A.D.

The time series modeling of 50-year tide gauge measurements has been carried out by using linear and smoothing spline methods with a 95% confidence interval.

For linear modelling, we supposed that the tide gauge measurement time series at time t_i is given by y_i, where i is the data number. Hence, the slope of tide gauge measurement time-series can be given by the following linear equation [17]:

$$y_i = a + bt \tag{1}$$

This kind of tide gauge modeling approach for sea-level data analysis is recognized as a linear fit. Here, the constants a and b are used to calculate the sea-level rising over the selected period. The estimated value of b is referred to as the slope of sea-level return.

TABLE 1. The PSMSL observation from six stations along the coastal area of the Gulf of Thailand.

PSMSL site name	Location	Data Availability	Rate of Change of Sea-level (mm/year)
POM PHRACHUN	13.550°N; 100.583°E	Jan 1971-Dec 2020	15.02
KO LAK	11.800°N; 99.817°E	Jan 1971-Dec 2020	3.39
KO MATTAPHON	10.450°N; 99.250°E	Jan 1992-Dec 2020	5.06
VUNGTAU	10.333°N; 107.067°E	Jan 1979-Dec 2018	3.73
GETING	6.226°N; 102.107°E	Jan 1987-Dec 2017	3.25
CENDERING	5.265°N; 103.187°E	Jan 1985-Dec 2018	3.19

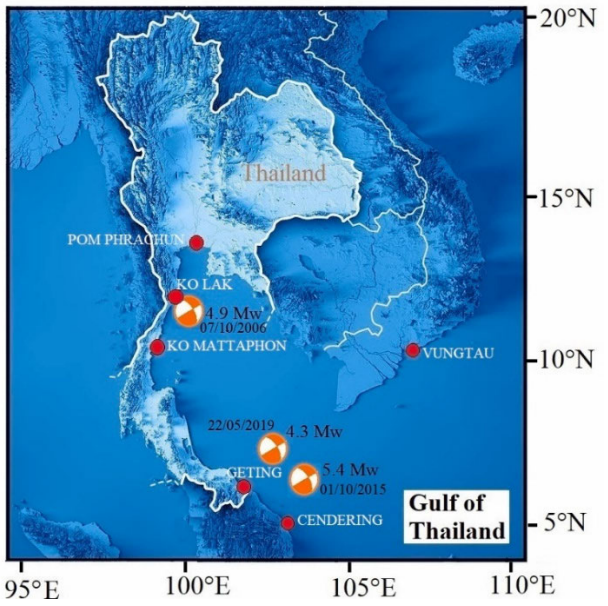

FIGURE 1. The PSMSL observation at six stations along the coastal area of the Gulf of Thailand during 1971 - 2020 A.D. The earthquake catalogs during 2005 - 2020 A.D. managed by the European–Mediterranean Seismological Centre (EMSC).

TABLE 2. The earthquake catalogs from 2005 to 2020 managed by the European–Mediterranean Seismological Centre (EMSC).

Date	Location	Earthquake Magnitude Scale (Mw)	Depth (km)	Region
2006-10-07	11.76°N; 100.06°E	4.9	34	Gulf of Thailand
2015-10-01	6.40°N; 103.50°E	5.4	10	Gulf of Thailand
2019-05-22	7.51°N; 102.38°E	4.3	10	Gulf of Thailand

Now, for smoothing spline modeling of y_i, we assumed there is a natural cubic spline function f(t_i) which contains an associated error (ε_i). Hence, the mathematical equation of this assumed function can be written like this [31]:

$$y_i = f(t_i) + \varepsilon_i \tag{2}$$

where $\varepsilon = (\varepsilon_1, \varepsilon_2, \ldots, \varepsilon_n)' \sim N(0, 1)$

This assumed natural cubic spline function f(t) in the close interval $[t_{i-1}, t_i]$, i=1, 2, 3, …n among n data points can be defined as follows:

$$f(t) = \begin{cases} f_0(t) = a_0 + b_0 t + c_0 t^2 + d_0 t^3 \\ \quad t \in [t_0, t_1] \\ f_1(t) = a_1 + b_1 t + c_1 t^2 + d_1 t^3 \\ \quad t \in [t_1, t_2] \\ \vdots \\ \vdots \\ f_{n-1}(t) = a_{n-1} + b_{n-1} t + c_{n-1} t^2 + d_{n-1} t^3 \\ \quad t \in [t_{n-1}, t_n] \end{cases} \tag{3}$$

where all a_i, b_i, c_i and d_i are 4n unknown constants. To estimate these the following 4n conditions are used:

$$\begin{aligned} f_i(t_{i+1}) &= f_{i+1}(t_{i+1}) \quad \text{for } 0 \le \text{i} \le \text{n-2} \\ f_i'(t_{i+1}) &= f_{i+1}'(t_{i+1}) \quad \text{for } 0 \le \text{i} \le \text{n-2} \\ f_i''(t_{i+1}) &= f_{i+1}''(t_{i+1}) \quad \text{for } 0 \le \text{i} \le \text{n-2} \\ f_0''(t_0) &= f_n''(t_n) = 0 \end{aligned} \tag{4}$$

Finally, we can estimate a smoothing spline function f_λ by minimizing:

$$\frac{1}{n}\sum_{i}^{n} (y_i - f(t_i))^2 + \lambda \int_0^{t_n} \left(f''(t)\right)^2 dt \tag{5}$$

Here the first term is used for fitting the curve and second term is used for smoothness. The parameter λ is known as a smoothing parameter for monitoring the trade-off between goodness-of-fit and smoothness of the estimates.

In the current study for numerical analysis a MATLAB tool (cftool) is used and their results are discussed in Section III (A). Here the known value λ will be chosen by MATLAB tool auomatically.

B. ANALYZING THE ORAS5 DATA

There are several studies based on tide gauge and altimetry have been carried out in several parts of the world [32], [33], [34]. They confirmed that the magnitude of change at the location of each tide gauge station was estimated using satellite altimetry measurements that agree with those from the tide-gauge data analysis. In the current analysis, we used some new kind of data known as Ocean Reanalysis System 5 (ORAS5) and excluded the altimetry data. This step analyzes the data from ORAS5 which is extracted from the latest ECMWF atmospheric reanalysis-ERA5 [35]. The ORAS5 production was a successor of ORAS4 [36] and has been funded by the Copernicus Climate Change Service (C3S). The model has many upgrades which include the prognostic thermodynamic-dynamic sea-ice model (LIM2) with the integration of sea-ice concentration data. The ORAS5 has an important novelty that provides explicitly the effect of surface wave's inclusion in the exchanging of momentum

and turbulent kinetic energy [37]. The spin-up strategy, an ensemble-based a priori bias scheme of correction, and the revised observation quality control (QC) procedures are some innovative features that are included in ORAS5. In the current study, the monthly ORAS5 data have been downloaded from the ECMWF atmospheric reanalysis-ERA5 site during 1971 - 2020 A.D. (https://cds.climate.copernicus.eu/cdsapp#!/dataset/reanalysis-oras5?tab=form) and the comparative analysis with PSMSL tide gauge sea-level has been done.

The observations obtained from the PSMSL tide gauge and the derived results of ORAS5 have different reference frames. Hence, for comparison analysis the separate means of both PSMSL and ORAS5 time-series are estimated and subtracted from their original time-series. Afterwards, we obtained two new time-series which are basically the deviations from their own means. The following mathematical methods are used for such kind of study:

$$\text{PSMSL}_{\text{New}} = \textit{mean}\ (\text{PSMSL}) - \text{PSMSL} \tag{6}$$

$$\text{ORAS5}_{\text{New}} = \textit{mean}\ (\text{ORAS5}) - \text{ORAS5} \tag{7}$$

Both the $\text{PSMSL}_{\text{New}}$ and the $\text{ORAS5}_{\text{New}}$ are the extacted time-series which are plotted in Fig. 3. These time-series are used for further comparative analysis.

C. APPLY MULTITAPER SPECTRAL ANALYSIS

Nowadays, the spectral analyses are regularly utilized in several fields such as the multi-decadal periodicities of tide gauge measurements [17]. There are several kinds of spectral analyses such as Lomb-scale, wavelet analysis, power spectrum, Welch method, and multitaper method [38], [39], [40] and they have their own benefits. For example, the wavelet analysis distinguishes amplitude and signal, while the multitaper method is very specific in frequency and less sensitive to weak signals and relies on finite observations that is widely applied in many fields such as the analysis of seismic data, radar ranging, and speech processing. Here, our step III proposed in this present work is based on the multitaper spectral analysis. A brief overview of the multitaper spectral analysis can be read additionally in Thomson [41].

Suppose there is a time-series of tide gauge measurement of N sample size with i^{th} tide gauge measurement given by y_i. The nonparametric estimates of the autocovariance sequence s_i can be obtained by using the most intuitive approach, namely moment method [42]

$$\hat{\mu} = \frac{1}{N}\sum_{k=0}^{N-1} y_k \tag{8}$$

$$\text{and } \hat{s}_i = \frac{1}{N}\sum_{k=0}^{N-i-1} \left(y_k - \hat{\mu}\right)\left(y_{k+i} - \hat{\mu}\right) \tag{9}$$

Then, we take the Fourier transform on both side of the above estimation, hence, we can obtain:

$$\hat{S}(f) = \Delta \sum_{i=-N+1}^{N-1} \hat{s}(i)\, e^{-2\pi ikf\Delta} = \frac{\Delta}{N}\left|\sum_{i=0}^{N-1} x_i e^{-2\pi ikf\Delta}\right| \tag{10}$$

The estimate of (10) is called the periodogram that can be calculated easily by using a program like MATLAB (e.g., https://ch.mathworks.com/help/signal/ref/pmtm.html).

III. RESULTS AND DISCUSSION

A. TIME-SERIES MODELLING OF PSMSL TIDE GAUGE

The time-series modeling of tide gauge measurement has been proposed by fitting the available data with linear and smoothing spline (non-linear) methods (Fig. 2). Decadal variation by using the monthly data has been shown on the x-axis, whereas the monthly mean sea-level (MSL) tide gauge variation (unit: meter) is plotted on the y-axis. The length of the dataset which was available at PSMSL is listed in Table 1. The respective equations for all tide sites have been shown in Fig. 2. A least square method is used to estimate the straight line in linear form. As we can see from the figure that the coefficient b is positive for all of them, this indicates the only rate of rising sea-level (no fall) measurement in the Gulf of Thailand. The MSL data at POM PHRACHUN with the data range between January 1971 and December 2020 has the highest rate of sea-level rising characterized by a slope of $b = 15.02$ mm/year. This is because this site is located near the Bay of Bangkok, where the Chao Phraya River and Tha Chin River become mainly empty. The tide gauge can affect these rivers because of the influences of moon and sun so that its water level characterized by periodic rise and fall [43]. The tidal river water level is mostly influenced by tides, waves, and overflow of rainfall [24]. Thus, the flood damage can be larger at high tide due to the effect of backwater. The MSL data at KO LAK with the data range between January 1971 and December 2020 also faced an earthquake event on October 7, 2006 and was characterized by a slope of $b = 3.39$ mm/year, with the Mw of 4.9 (Fig. 1). There is a break rise and a fall is also clearly visible from the figure but it's very difficult to conclude whether this break occurred because of this small earthquake or not. This is because the available data is the monthly average, and the earthquake influence disappeared in a few days. The MSL data at KO MATTAPHON with the data range between January 1992 and December 2020 was characterized by a slope of $b = 5.06$ mm/year. This is the second-highest rate of change in sea level among the six selected tide gauge sites of this present study. This rate is high because the Tha Taphap River is becoming empty in this region. The whole list of rates of change in sea-level has been given in Table 1. As we can see from the table that the average rate of change of other sites is almost 3.5 mm/year (with little up and down). These fluctuations in the rate of change can be related to the depth of water, the shape of the ocean floor (bathymetry), the shape of

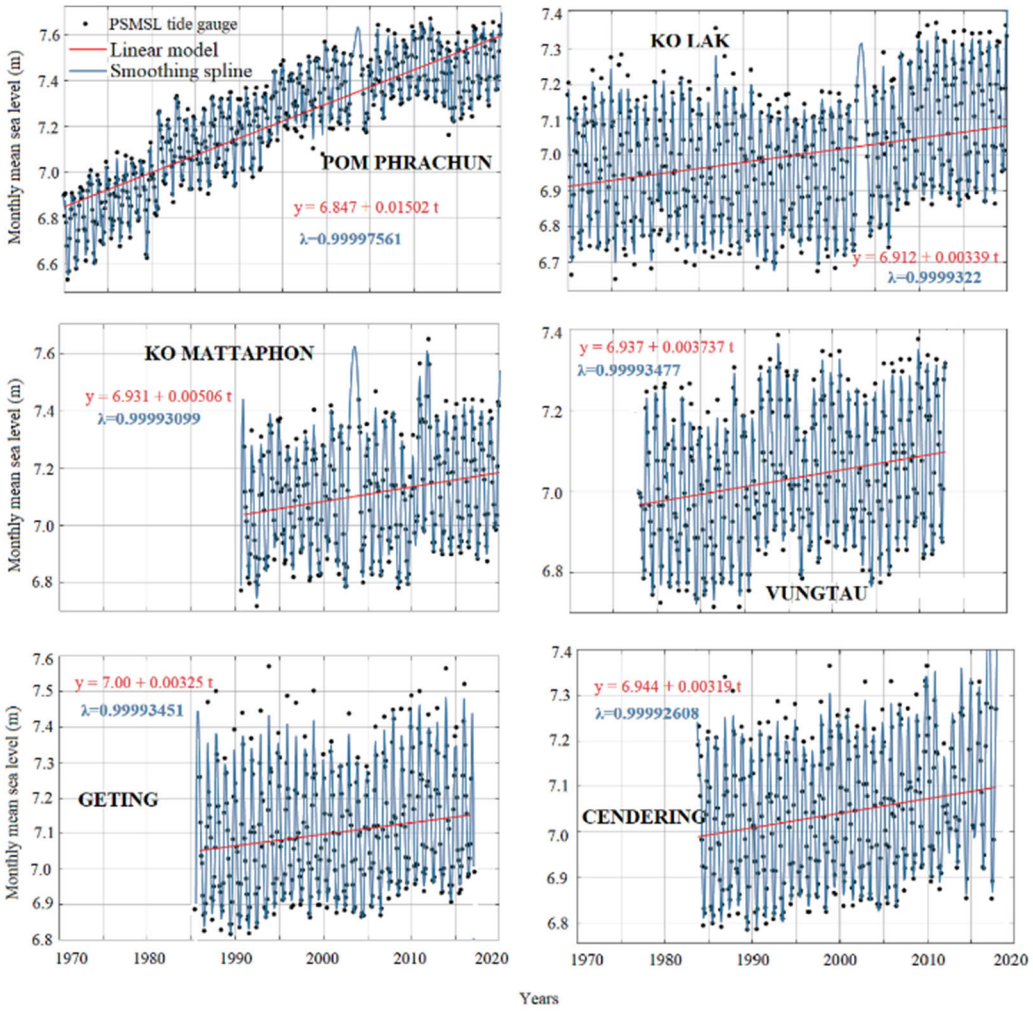

FIGURE 2. The time-series modeling of 50-year tide gauge measurements carried out by using linear and smoothing spline methods at six sites along the coastal area of the Gulf of Thailand.

the land, the restrictions to flow (e.g., narrow inlets to bays), and the local wind, etc. There are two earthquake events that have been recorded on October 1, 2015 (Mw 5.4) and May 22, 2019 (Mw 4.3). Although the earthquake events seem to be responsible for the rising and fall of tide gauge measurement, but their influence because of lack of data cannot be given scientifically.

The tide gauge data have been modeled by the smoothing spline method and their smoothing parameters (λ) are also indicated in the respective sites. The tide gauge data at POM PHRACHUN have been fitted by the smoothing spline method where the smoothing parameter is very high ($\lambda = 0.99997561$) indicating the best fitting of the tide gauge data. The modeled data filled the gaps available in the record and reduced the influence of noise error in the available dataset. The data which contain noise error are not touched by the smoothing curve. In this way, the impact of real-time rising and fall or a kind of tidal cycle of the sea-level surface is clearly visible from the smoothing curves. This happens because the ocean is affected by the experience of the earth-moon system with the new tidal cycle every 27.3 days and both the moon, and the earth revolve around a common point at every 27.3 days. There is a high and low tidal cycle which can also be seen from the smoothing curves that happens because the distance change between the earth and the moon. The tide gauge data at KO LAK have been fitted by the smoothing spline method in which the smoothing parameter is very high ($\lambda = 0.9999322$) that also indicate the best fitting of the tide gauge data. The other definition regarding the tidal cycle of KO LAK is similar to that of POM PHRACHUN and belongs to the earth-moon system tidal cycle every 27.3 days. The list of smoothing parameters at each site is given in Table 3.

As for Table 3, the values of these smoothing parameters at each site are very high (more than 0.999) indicating the best fitting of the tide gauge data and the influence of noise error in the available dataset. To understand the influence and the relation between the smoothing spline modeled tide data and

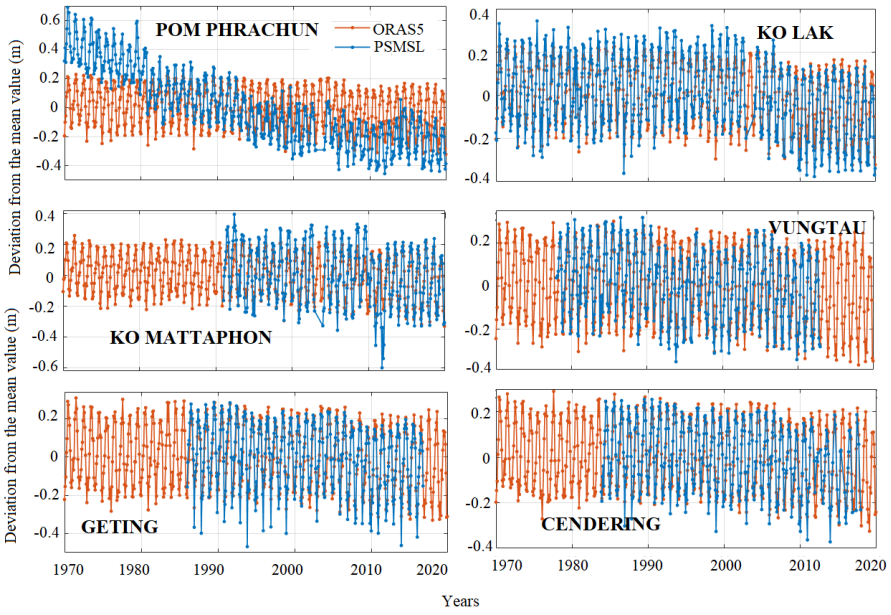

FIGURE 3. The comparisons of the new estimated time series of both PSMSL and ORAS5 tide gauge datasets at six sites.

TABLE 3. The list of smoothing parameters of each site. The correlation coefficient and RMSE smoothing spline modeled tide data and observed tide gauge data.

PSMSL tide gauge site name	Smoothing parameter (λ)	Correlation Coefficient	RMSE (meter)
POM PHRACHUN	0.99997561	0.9974	0.03546
KO LAK	0.99993220	0.9875	0.04281
KO MATTAPHON	0.99993099	0.9889	0.04597
VUNGTAU	0.99993477	0.9896	0.03744
GETING	0.99993451	0.9864	0.04540
CENDERING	0.99992608	0.9897	0.03410

the observed tide gauge data, the correlation coefficient and the root mean square error (RMSE) are estimated between them as shown in Table 3. As we can see from the table that all correlation coefficients are greater than 0.985 with a maximum value of 0.9974. This means that they are well correlated and approved the efficiency of the smoothing spline method. The list of RMSE values between the observed and the modeled datasets are also shown in Table 3. The RMSE values are very low between 0.0341 m and 0.04597 m. This also approves the suitability of the smoothing spline method employed in this present work.

B. COMPARISON WITH ORAS5

The observations obtained from PSMSL tide gauge sea level is compared to the tide gauge benchmark, while the derived results of ORAS5 are compared to their own reference. Therefore, a mean sea level is achieved by using Equations (6) and (7), and two new time series are estimated for the comparison of both datasets as plotted in Fig. 3. The PSMSL tide gauge data are derived and shown with the blue lines, while the ORAS5 ones are depicted with the orange lines. In Fig. 3, the observation dates are shown by the horizontal axis, while the new estimated time series of both PSMSL and ORAS5 observations are presented by the vertical axis. There is a significant role of the monthly periodicity in sea level like the original PSMSL and it is clearly visible from both time series that there is no property change of each observation. Moreover, the small variations between both datasets are available at POM PHRACHUN, while the good agreements between both time-series estimates over a period of available datasets can be seen among other sites. As discussed earlier, the rate of sea-level rising at POM PHRACHUN is very high because of the influence of local rivers. The ORAS5 data is a modeled dataset, hence, it might not model the local influence. On the other hand, all other sites show very good agreements, since they are not affected significantly by the local influence. Note that the PSMSL tide gauge measurements have missing values, while the ORAS5 tide gauge measurements have all values. To correlate both datasets, the ORAS5 tide gauge measurements values which were not timely matching with the PSMSL datasets are excluded.

The correlation coefficients and the RMSEs between them are estimated and showed in Table 4. It is visible from Table 4 that the correlation coefficient and the RMSE value at POM PHRACHUN site are equal to 0.5446 and 0.21614 m, respectively. These values indicate that both datasets are not well correlated as expected because of the influence of local rivers. The results also show that the correlation coefficients at both KO MATTAPHON and VUNGTAU sites are equal to 0.8905 and 0.8721, respectively. We already discussed that the Tha Taphap River becoming empty at KO MATTAPHON

TABLE 4. The correlation coefficient and the RMSE (unit: meter) between PSMSL and ORAS5 datasets.

PSMSL tide gauge site name	Correlation Coefficient	RMSE (meter)
POM PHRACHUN	0.5446	0.21614
KO LAK	0.9371	0.06389
KO MATTAPHON	0.8905	0.09665
VUNGTAU	0.8721	0.08521
GETING	0.9432	0.05832
CENDERING	0.9412	0.18499

makes some local influence and creates some errors in the ORAS5 datasets. Similarly, the VUNGTAU which basically located in the East Vietnam Sea is also affected by the local rives such as the Co Cochien River, the Ham Luong River, Mekong River, and Soai Rap, etc. As for the KO LAK, GETING, and CENDERING sites, the correlation coefficients between both datasets are equal to 0.9371, 0.9432, and 0.9412, respectively, and their RMSEs are equal to 0.06389 m, 0.05832 m, and 0.18499 m, respectively. These correlation coefficients are quite high (more than 0.90) and these RMSEs are very low. These values indicates that if there is no local influence, the ORAS5 is able to provide a new chance to monitor sea-level changes with the available datasets.

To show the cross spectra (coherence and phase) of the measured sea level data and the ORAS5 data, we studied magnitude-squared coherence and cross spectrum phase with 95% confidence intervals and displayed in Fig.4a and Fig. 4b. The coherence is the normalized cross-spectrum and takes values between 0 and 1. However, it is computed by taking the square value of the cross-spectrum, which deletes information about the phase of the two signals. The coherence tells you how strong the correlation between two signals is, and if we have two noisy measurements, it will tell us if there is any underlying low strength signal, they have in common. Whereas the cross-spectrum can help to understand how their phases are related. The signals in phase the cross-spectrum will be positive, if they are ± 180 deg out of phase the cross-spectrum will be negative. In fact, the cross-spectrum will be positive values for a phase shift between 0° to 90°, negative values between 90° to 270° and again positive values between 270° to 360°. The coherence function is a measure based upon the auto- and cross-spectral properties of two processes. Its definition is identical in form to the square of a correlation coefficient between the spectral components of the processes at a particular frequency f. As we can see from Fig. 4a, the frequency where both time-series (PSMSL and ORAS5) are identical processes, then their power spectra are equal to each other and to the cross spectrum. In this case, the coherence is 1 at all frequencies. And if both time-series (PSMSL and ORAS5) are completely independent processes, then the cross spectrum is 0 for all frequencies and so is the coherence. Between these two extremes lies a range of possible relationships between the two processes that can be measured by the coherence function. Regarding Fig. 4b, if the processes PSMSL and OARS5 are uncorrelated, then no particular relative phase relationship is to be expected at any frequency. Relative phase will be a random variable with 0 mean and uniformly distributed over the range -90 to $+90$ degrees. When there is a correlation between the two processes, the relative phase relation is showing up as a preferred relative phase angle related to frequency. A significant coherence value indicates that the relative phase is concentrated around the mean. If it is not significant, then the relative phase distribution is not significantly concentrated, and the mean relative phase will not be meaningful. It can be noted from the Fig. 4b, that the phase confidence limits are small where the coherence magnitude is large. The confidence interval for the amplitude can rise above the level-of-no-significance even when the estimated value is itself below the level

C. MULTITAPER SPECTRAL ANALYSIS

In the above study, we discussed the sea-level trend observed at different sites in the Gulf of Thailand and got a rough idea that the trend of the POM PHRACHUN site is different as compared to that of other sites. As described earlier, there is a small-level variation at each site because of local influence which cannot be recognized by the above analysis. To examine the performance and the complexity of the tide gauge measurements, the multitaper spectral analysis from four out of six stations (no need to show all of them because of almost the same properties) is applied and the spectral estimates with 95% confidence bounds are estimated on a linear-linear scale as shown in Fig. 5. The complete analysis of multitaper spectral analysis is carried out by using MATLAB code that can be accessible via https://ch.mathworks.com/help/signal/ref/pmtm.html. To obtain the multitaper power spectral density (PSD) estimates, the monthly measurement is sampled with 100 Hz trigonometric function sine wave and the additive white Gaussian noise N(0,1). Here we set the window length to 600 samples (the monthly 50-year observations will contain 600 data). This window length contains 60 periods of the 600 Hz sine wave. Input the sample rate explicitly to get the output frequencies in Hz (1/month).

As we can see in Fig. 1, only two sites (i.e., POM PHRACHUN and KO LAK) have PSMSL full data, hence, these two sites are selected for multitaper spectral analysis and illustrated with the blue lines in Fig. 5. The other two sites (i.e., GETING and CENDERING) from the ORAS5 dataset that correlate with the corresponding PSMSL with the correlation coefficients of more than 0.94 are selected and showed with the orange lines in Fig. 5. The power/frequency (unit: dB/Hz) values estimated by multitaper spectral analysis have been plotted on the vertical axis, while the horizontal axes present the frequency (unit: 1/month). All the estimated density plots of multitaper spectral analysis are plotted in the range between -90 dB/Hz and 10 dB/Hz. Since the PSD estimation uses a time-half bandwidth, hence, its length

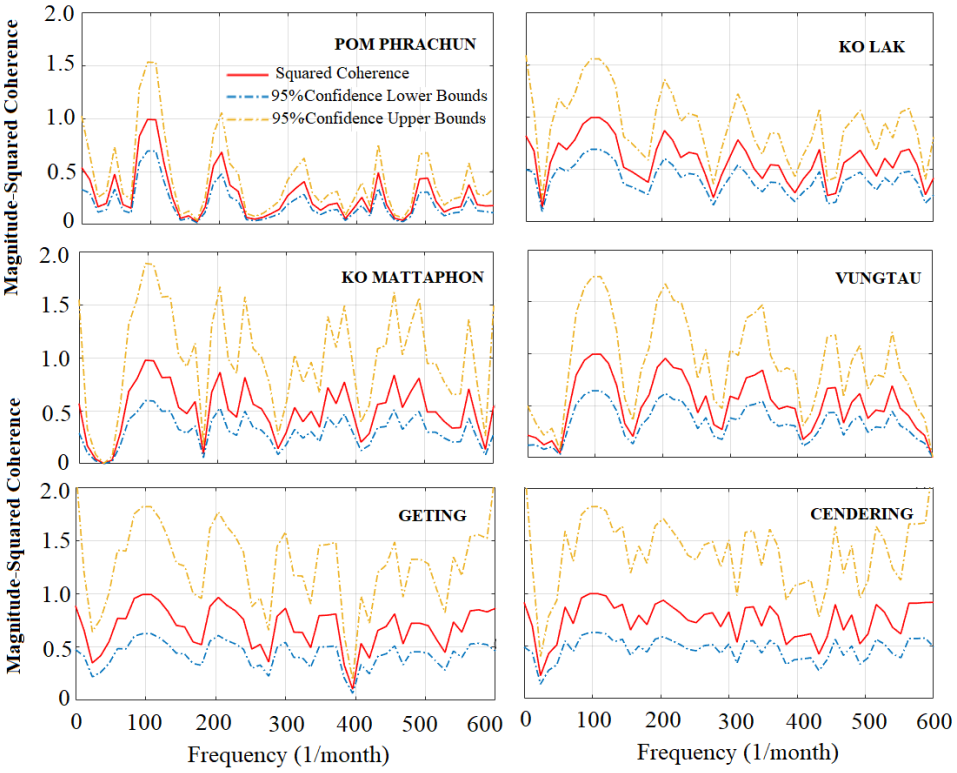

(a)

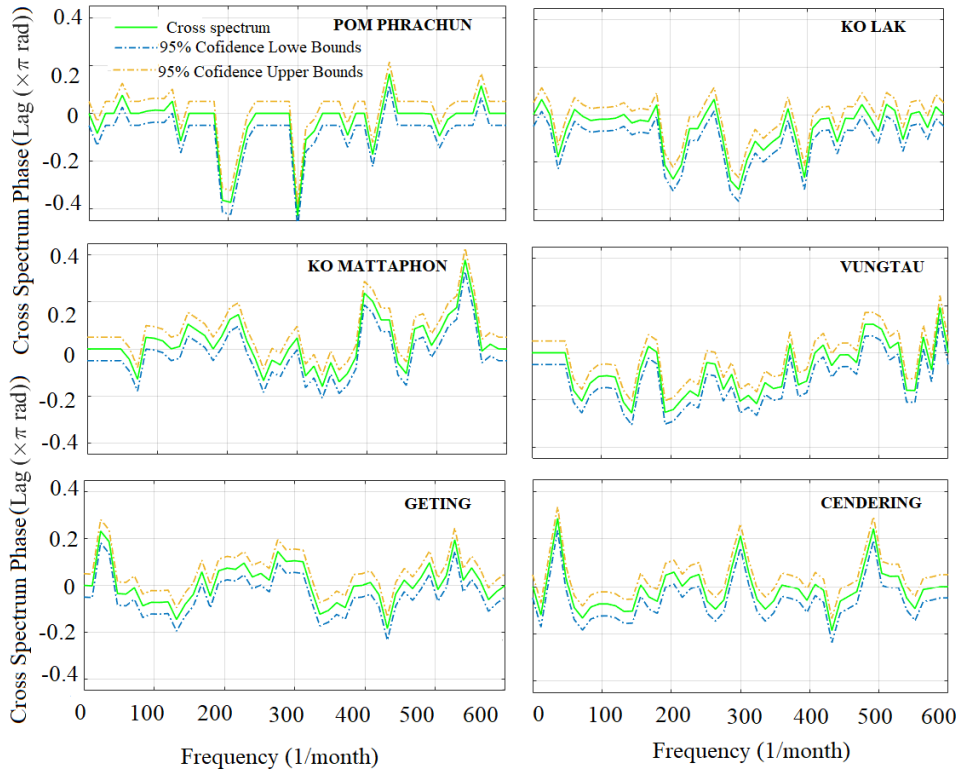

(b)

FIGURE 4. (a) Squared Coherence Analysis between the times series of PSMSL and ORAS5 with 95% Confidence Bounds. (b) Cross spectrum Phase Analysis between the times series of PSMSL and ORAS5 with 95% Confidence Bounds.

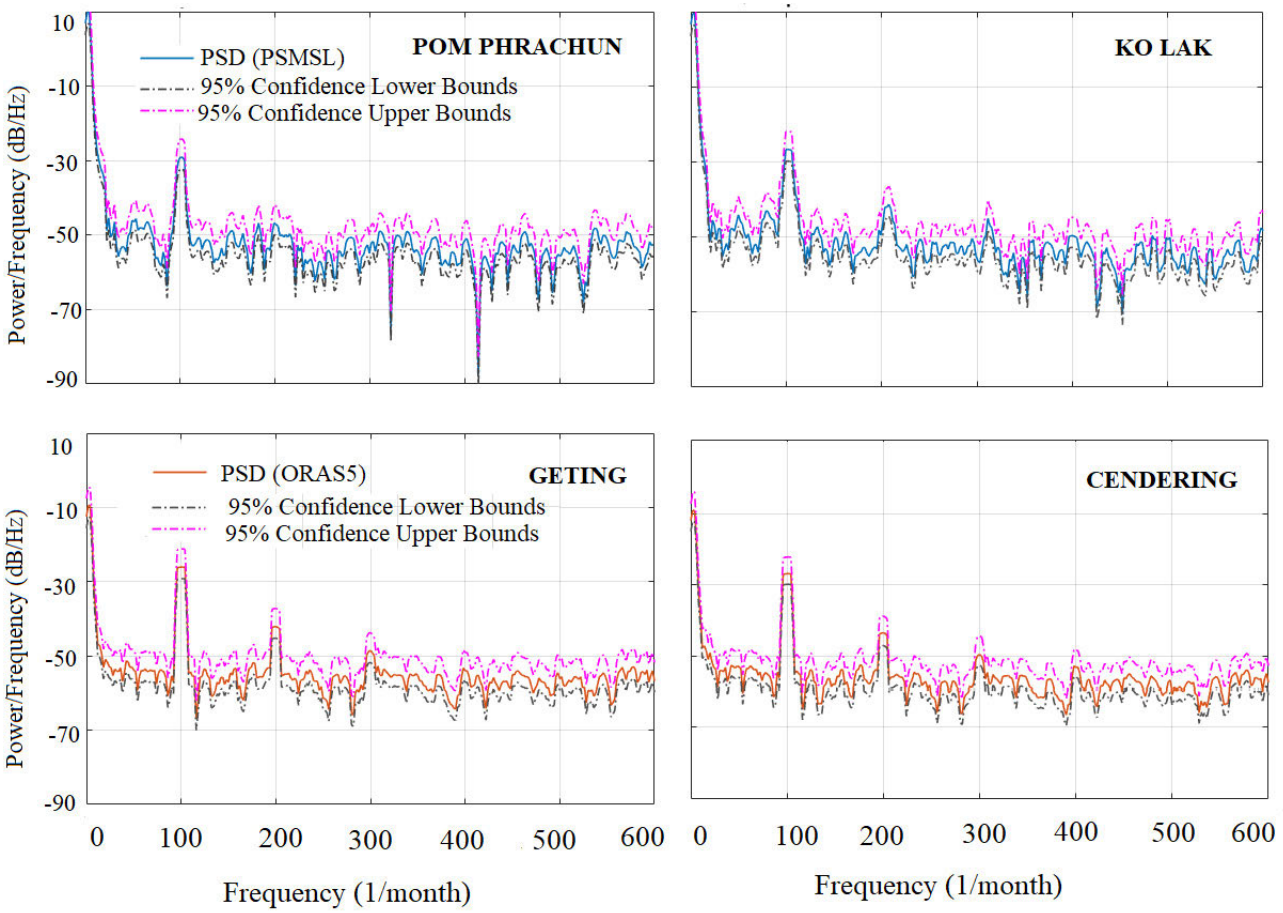

FIGURE 5. The multitaper spectral analysis and the spectral estimates with 95% confidence bounds in forms of linear-linear scale at four sites (i.e., POM PHRACHUN, KO LAK, GETING, and CENDERING).

is double the number of measurements, i.e., the monthly 50-year observations in this present work have 600 data. In this way, it is very easy to recognize the peak in the frequency band. As we can see from the figure that the first peak is clearly visible at 100 Hz at each site. At a first glance of these density plots, we can say that the tide gauge trends at the considered sites differ one another and they can be used to differ the sea-level change and their own characterizations. Different tide gauge performances can be expected because the tide gauge sites are affected due to some local influences. As shown in Fig. 5, the POM PHRACHUN does not have a second peak at 200 Hz, while other sites have a second peak with high or low magnitude. This happens because the POM PHRACHUN site is affected by the influence of local rivers as they can be seen obviously by the multitaper PSD function. If we roughly talk about the differences between the other three sites (i.e., KO LAK, GETTING and CENDERING), they have the first two common peaks at 100 and 200 Hz, while the third peak is invisible at KO LAK site, this is because the trend of KO LAK shows a break in time series between the year 2000 and 2005. In general, these results point out that the peak variations of multitaper PSD function are different one another. This means that the sea-level measurements at different sites have different periodic variations with different levels of fluctuation. In summarized way, we can say that the multitaper spectral analysis evidently show the differences between the sea-level performance and can be applied to attain the overall periodic fluctuation level of the water surface.

IV. CONCLUSION

The study investigates the tide gauge data at six sites located around the coastal area of the Gulf of Thailand. Both linear and non-linear (smoothing spline) modelling based on PSMSL tide gauge data are carried out and the modeled data are compared with the ORAS5 tide gauge measurements. The conclusion of the study are as follows:

1. The mean sea-level (MSL) at POM PHRACHUN site shows the highest rate ($b = 15.02$ mm/year) of sea-level rising. The main reason is due to the impacts of the local rivers located near the Bay of Bangkok where Chao Phraya River and Tha Chin River become mainly empty.

2. The tide gauge data modeled by the smoothing spline method shows very high smoothing parameter ($\lambda > 0.999$) that indicates the best fitting of the tide gauge data and approves the efficiency of the smoothing spline method.
3. The correlation coefficients between PSMSL and ORAS5 tide gauges are quite high (more than 0.90) and the RMSE values are very low. These indicators show manifestly that the ORAS5 is able to provide a new chance to monitor sea-level changes with the available datasets.
4. Finally, the multitapers spectral analysis is used to examine the performance and the complexity of the tide gauge measurements. Our studied results show that the multitapers spectral analysis can be applied to attain the overall periodic sea-level fluctuation over the globe.

ACKNOWLEDGMENT

The authors would like to thank to the Permanent Service for Mean Sea Level (PSMSL) for the mean sea level data and the European–Mediterranean Seismological Centre (EMSC) for the earthquake data and also would like to express the gratitude to The Ocean Reanalysis System 5 (ORAS5) for the tide gauge sea level data and the Wikipedia for the details of the Gulf of Thailand.

REFERENCES

[1] J. A. Church and N. J. White, "A 20th century acceleration in global sea-level rise," *Geophys. Res. Lett.*, vol. 33, no. 1, pp. 1–4, Jan. 2006.

[2] A. Parker, "Apparent hot and cold spots of acceleration along the Atlantic and Pacific coasts of the United States," *Nonlinear Eng.*, vol. 3, no. 1, pp. 51–56, Mar. 2014.

[3] Y. N. Sasaki, R. Washizu, T. Yasuda, and S. Minobe, "Sea level variability around Japan during the twentieth century simulated by a regional ocean model," *J. Climate*, vol. 30, no. 14, pp. 5585–5595, Jul. 2017.

[4] X. Chen, B. Qiu, S. Chen, and Y. Qi, "Period-lengthening of the Mindanao current variability from the long-term tide gauge sea level measurements," *J. Geophys. Res., Oceans*, vol. 126, no. 8, Aug. 2021, Art. no. 2020JC016932.

[5] D. T. Pugh, *Tides, Surges and Mean Sea Level*. Hoboken, NJ, USA: Wiley, 1987.

[6] G. Jordà, D. Gomis, E. Álvarez-Fanjul, and S. Somot, "Atmospheric contribution to Mediterranean and nearby Atlantic Sea level variability under different climate change scenarios," *Global Planet. Change*, vols. 80–81, pp. 198–214, Jan. 2012.

[7] A. H. Sallenger, K. S. Doran, and P. A. Howd, "Hotspot of accelerated sea-level rise on the Atlantic coast of North America," *Nature Climate Change*, vol. 2, no. 12, pp. 884–888, Dec. 2012.

[8] A. M. Radwan, M. Magdy, M. Rabah, A. Saber, and A. Zaki, "Sea level analysis using tide gauge observations at the northern delta coast, Egypt," *NRIAG J. Astron. Geophys.*, vol. 10, no. 1, pp. 361–371, Jan. 2021.

[9] K. Ansari, "Modelling and spectral analysis of sea-level trend over Indian coastal area," *Mar. Geophys. Res.*, vol. 43, no. 1, pp. 1–9, Mar. 2022.

[10] T. Suzuki and M. Ishii, "Regional distribution of sea level changes resulting from enhanced greenhouse warming in the model for interdisciplinary research on climate version 3.2," *Geophys. Res. Lett.*, vol. 38, no. 2, pp. 1–6, Jan. 2011.

[11] N. L. Bindoff, J. Willebrand, V. Artale, A. Cazenave, J. M. Gregory, S. Gulev, K. Hanawa, C. Le Quere, S. Levitus, Y. Nojiri, and C. K. Shum, "Observations: Oceanic climate change and sea level," in *Climate Change 2021: The Physical Science Basis* (Contribution of Working Group I), Solomon, Ed. Cambridge, U.K.: Cambridge Univ. Press, 2007, pp. 385–428.

[12] K. Ansari and T.-S. Bae, "Modelling and mitigation of real-time sea level measurement over the coastal area of Japan," *Mar. Geophys. Res.*, vol. 42, no. 4, pp. 1–15, Dec. 2021.

[13] X. Zhang and J. A. Church, "Sea level trends, interannual and decadal variability in the Pacific ocean," *Geophys. Res. Lett.*, vol. 39, no. 21, pp. 1–8, Nov. 2012.

[14] A. Timmermann, S. McGregor, and F.-F. Jin, "Wind effects on past and future regional sea level trends in the southern indo-Pacific," *J. Climate*, vol. 23, no. 16, pp. 4429–4437, Aug. 2010.

[15] Y. N. Sasaki, S. Minobe, N. Schneider, T. Kagimoto, M. Nonaka, and H. Sasaki, "Decadal sea level variability in the south Pacific in a global eddy-resolving ocean model hindcast," *J. Phys. Oceanogr.*, vol. 38, no. 8, pp. 1731–1747, Aug. 2008.

[16] P. D. Bromirski, A. J. Miller, R. E. Flick, and G. Auad, "Dynamical suppression of sea level rise along the Pacific coast of North America: Indications for imminent acceleration," *J. Geophys. Res., Oceans*, vol. 116, no. C7, pp. 1–13, Jul. 2011.

[17] A. Parker, "Sea level oscillations in Japan and China since the start of the 20th century and consequences for coastal management—Part 2: China pearl river delta region," *Ocean Coastal Manage.*, vol. 163, pp. 456–465, Sep. 2018.

[18] R. J. Nicholls and A. Cazenave, "Sea-level rise and its impact on coastal zones," *Science*, vol. 328, no. 5985, pp. 1517–1520, 2010.

[19] A. Ranjbar, C. Cherubini, and A. Saber, "Investigation of transient sea level rise impacts on water quality of unconfined shallow coastal aquifers," *Int. J. Environ. Sci. Technol.*, vol. 17, no. 5, pp. 2607–2622, May 2020.

[20] N. Schaefer, M. Mayer-Pinto, K. J. Griffin, E. L. Johnston, W. Glamore, and K. A. Dafforn, "Predicting the impact of sea-level rise on intertidal rocky shores with remote sensing," *J. Environ. Manage.*, vol. 261, May 2020, Art. no. 110203.

[21] W. Shi, C. Lu, and A. D. Werner, "Assessment of the impact of sea-level rise on seawater intrusion in sloping confined coastal aquifers," *J. Hydrol.*, vol. 586, Jul. 2020, Art. no. 124872.

[22] S. Kang and H. Lin, "Wavelet analysis of hydrological and water quality signals in an agricultural watershed," *J. Hydrol.*, vol. 338, nos. 1–2, pp. 1–14, May 2007.

[23] H. Hidayat, A. J. F. Hoitink, M. G. Sassi, and P. J. J. F. Torfs, "Prediction of discharge in a tidal river using artificial neural networks," *J. Hydrologic Eng.*, vol. 19, no. 8, Aug. 2014, Art. no. 04014006.

[24] M. Lee, Y. You, S. Kim, K. Kim, and H. Kim, "Decomposition of water level time series of a tidal river into tide, wave and rainfall-runoff components," *Water*, vol. 10, no. 11, p. 1568, Nov. 2018.

[25] A.-L. Balogun and N. Adebisi, "Sea level prediction using ARIMA, SVR and LSTM neural network: Assessing the impact of ensemble ocean-atmospheric processes on models' accuracy," *Geomatics, Natural Hazards Risk*, vol. 12, no. 1, pp. 653–674, Jan. 2021.

[26] J. S. Deepa and C. Gnanaseelan, "The decadal sea level variability observed in the Indian ocean tide gauge records and its association with global climate modes," *Global Planet. Change*, vol. 198, Mar. 2021, Art. no. 103427.

[27] V. Piscopo, G. B. Rossi, F. Crenna, S. Gaglione, A. Scamardella, M. Uttieri, and E. Zambianchi, "Measurement of sea waves," in *Measurement for the Sea*. Cham, Switzerland: Springer, 2022, pp. 157–179.

[28] M. Beenstock, D. Felsenstein, E. Frank, and Y. Reingewertz, "Tide gauge location and the measurement of global sea level rise," *Environ. Ecol. Statist.*, vol. 22, no. 1, pp. 179–206, Mar. 2015.

[29] G. T. Mitchum, R. S. Nerem, M. A. Merrifield, and W. R. Gehrels, "Modern sea-level-change estimates," in *Understanding Sea-Level Rise and Variability*. Hoboken, NJ, USA: Blackwell, Jul. 2010, pp. 122–142, doi: 10.1002/9781444323276.ch5.

[30] B. C. Douglas, "Sea level change in the era of the recording tide gauge," *Int. Geophys.*, vol. 75, pp. 37–64, Jan. 2001.

[31] Y. Wang, "Smoothing spline models with correlated random errors," *J. Amer. Stat. Assoc.*, vol. 93, no. 441, pp. 341–348, Mar. 1998.

[32] G. Wöppelmann and M. Marcos, "Coastal sea level rise in southern Europe and the nonclimate contribution of vertical land motion," *J. Geophys. Res., Oceans*, vol. 117, no. C1, pp. 1–14, Jan. 2012.

[33] N. B. Avsar, S. Jin, H. Kutoglu, and G. Gurbuz, "Sea level change along the black sea coast from satellite altimetry, tide gauge and GPS observations," *Geodesy Geodynamics*, vol. 7, no. 1, pp. 50–55, Jan. 2016.

[34] H. Taibi and M. Haddad, "Estimating trends of the Mediterranean Sea level changes from tide gauge and satellite altimetry data (1993–2015)," *J. Oceanol. Limnol.*, vol. 37, no. 4, pp. 1176–1185, Jul. 2019.

[35] H. Zuo, M. A. Balmaseda, K. Mogensen, and S. Tietsche, "OCEAN5: The ECMWF ocean reanalysis system and its real-time analysis component," Eur. Centre Medium-Range Weather Forecasts, Reading, U.K., Tech. Rep. 823, 2018.
[36] M. A. Balmaseda, K. Mogensen, and A. T. Weaver, "Evaluation of the ECMWF ocean reanalysis system ORAS4," *Quart. J. Roy. Meteorological Soc.*, vol. 139, no. 674, pp. 1132–1161, Jul. 2013.
[37] Ø. Breivik, K. Mogensen, J. Bidlot, M. A. Balmaseda, and P. A. E. M. Janssen, "Surface wave effects in the NEMO ocean model: Forced and coupled experiments," *J. Geophys. Res., Oceans*, vol. 120, no. 4, pp. 2973–2992, Apr. 2015.
[38] N. R. Lomb, "Least-squares frequency analysis of unequally spaced data," *Astrophys. Space Sci.*, vol. 39, no. 2, pp. 447–462, Feb. 1976.
[39] M. K. Van Vugt, P. B. Sederberg, and M. J. Kahana, "Comparison of spectral analysis methods for characterizing brain oscillations," *J. Neurosci. Methods*, vol. 162, nos. 1–2, pp. 49–63, May 2007.
[40] K. Ansari and T. Bae, "Wavelet and power spectrum analysis of global navigation satellite system multipath error modeling and mitigation," *Int. J. Satell. Commun. Netw.*, vol. 39, no. 6, pp. 626–644, Nov. 2021.
[41] D. J. Thomson, "Spectrum estimation and harmonic analysis," *Proc. IEEE*, vol. 70, no. 9, pp. 1055–1096, Sep. 1982.
[42] B. Babadi and E. N. Brown, "A review of multitaper spectral analysis," *IEEE Trans. Biomed. Eng.*, vol. 61, no. 5, pp. 1555–1564, May 2014.
[43] F. A. Buschman, A. J. F. Hoitink, M. Van Der Vegt, and P. Hoekstra, "Subtidal water level variation controlled by river flow and tides," *Water Resour. Res.*, vol. 45, no. 10, pp. 1–12, Oct. 2009.

KUTUBUDDIN ANSARI received the Ph.D. degree from the Indian Institute of Technology Bombay, India, in 2014, through the GPS Geodesy. Since 2020, he has been working as the Managing Director of Integrated Geoinformation (IntGeo) Solution Private Ltd., New Delhi, India. His research interests include GNSS-based geodesy, atmospheric and oceanic technology, and real-time positioning based on multi-constellation GNSSs.

JOSÉ FRANCISCO DE OLIVEIRA-JÚNIOR received the bachelor's degree in meteorologia and the master's degree in geosciences from the Universidade Federal de Alagoas, Brazil, in 1998 and 2001, respectively, the Ph.D. degree in meteorology from the Instituto Nacional de Pesquisas Espaciais, in 2003, and the Ph.D. degree in civil engineering from the Universidade Federal do Rio de Janeiro, in 2008. He has worked as an Associate Professor with the Instituto de Ciências Atmosféricas, Universidade Federal de Alagoas. He has experienced in geosciences, especially micrometeorology and acted on the following subjects, such as camada limite atmosferica, estatística, modelagem, and alagoas and camada limite atmosférica.

PUNYAWI JAMJAREEGULGARN received the Ph.D. degree from the Department of Telecommunication Engineering, King Mongkut's Institute of Technology Ladkrabang, Bangkok, Thailand, in 2017. Since 2012, he has been working as an Associate Professor with the Department of Engineering, King Mongkut's Institute of Technology Ladkrabang, Prince of Chumphon Campus, Chumphon, Thailand. His research interests include ionospheric irregularities, TEC modeling, RTK-based positioning and multi-GNSS signals, plasma bubbles, and earthquake investigations based on GPS TEC and GIM TEC.